

**Influence of spherical anisotropy on optical mass sensing in plasmonic-molecular optomechanics**Elnaz Aleebrahim,<sup>1</sup> Malek Bagheri Harouni <sup>1,2,\*</sup> and Ehsan Amooghorban <sup>3,4,†</sup><sup>1</sup>*Department of Physics, University of Isfahan, Hezar Jerib Street, Isfahan 81764-73441, Iran*<sup>2</sup>*Quantum Optics Group, Department of Physics, University of Isfahan, Hezar Jerib Street, Isfahan 81764-73441, Iran*<sup>3</sup>*Department of Physics, Faculty of Basic Sciences, Shahrekord University, P.O. Box 115, Shahrekord 88186-34141, Iran*<sup>4</sup>*Photonic Research Group, Shahrekord University, Shahrekord 88186-34141, Iran*

(Received 27 February 2022; accepted 13 June 2022; published 30 June 2022)

We use an all-optical pump-probe method to develop a mass-sensing mechanism in a molecular plasmonic system at room temperature. The system consists of a doubly clamped graphene nanoribbon that parametrically interacts with two types of isotropic and anisotropic spherical plasmonic cavities in the presence of a strong pump field and a weak probe pulse. Based on the mode-selective quantization scheme and analogy with the canonical model of the cavity optomechanics, we formulate the Hamiltonian of the system in terms of the electromagnetic Green's tensor. In this manner, we derive an explicit form of the size-dependent optomechanical coupling function and plasmonic damping rate, which include the modal, geometrical, and material features of the plasmonic structure. Engineering material features of the plasmonic nanostructure, we find that the intensity of the probe-field transmission spectrum for radially anisotropic spherical nanocavity is enhanced significantly compared to the silver sphere nanocavity due to the mode volume reduction. This scheme can allow us to achieve the minimum measurable mass  $\Delta m \approx 10^{-24}$  kg at room temperature.

DOI: [10.1103/PhysRevA.105.062609](https://doi.org/10.1103/PhysRevA.105.062609)**I. INTRODUCTION**

One of the most promising methods for tailoring light-matter interaction is to employ metallic structures of nanoscale size as plasmonic nanocavities [1–6]. Localized plasmon resonances (LPRs), which result from the confinement of light waves within the metallic subwavelength structures, are considered as the fundamental concept of a new growing field known as plasmonic cavity quantum electrodynamics (PCQED) [7–9]. These localized plasmons can be effectively controlled by adjusting cavity composition, size, and shape and the material parameters of the surrounding medium. The sub-diffraction-limit focusing of electromagnetic fields in the near field of the LPRs is responsible for the enormous enhancement of the Raman spectrum in a common sensing technique known as surface-enhanced Raman scattering (SERS) [10]. So far, the dynamical behavior of SERS phenomenon, which represents the interaction between molecular species and metallic nanoparticles, was formulated theoretically in the field of molecular plasmonic in both classical and quantum regimes [1,3,5,11]. Many attempts have been devoted to investigating the influence of material and geometrical parameters such as anisotropy on the SERS enhancement factor by finding the scalar potential distribution of the nanostructure and extracting its polarizability in the quasistatic approximation (QSA) [12].

Recently, a theoretical approach was introduced to explain the dynamical nature of plasmon-phonon interaction by

mapping the molecular plasmonic system onto the canonical model of cavity optomechanics [13]. Based on this model, it was shown that the polarizability of the molecule and its interaction with a plasmonic nanocavity are explicitly dependent on the internal vibrational states of the adjacent molecule [14,15]. This theoretical approach was applied to the SERS phenomenon and successfully described fundamental classical properties such as the dependence of the Raman signal on the intensity and frequency of the incident laser. Quantum features like dynamical backaction amplification, which are related to the vibrational modes and correlations between emitted photons of the molecules, can be described through the molecular optomechanical model [14–17].

Several challenging phenomena such as distinguishing similar molecules and designing tunable optical switches have been studied in this framework [18]. Heat transfer of two adjacent molecules in a plasmonic nanocavity, optomechanical cooling in the nonlinear regime, collective effects in SERS, and optical mass sensing are other noticeable phenomena that have recently been investigated through this optomechanical model [12,18–21].

Zhu and co-workers proposed recently a mass-sensing setup with high precision at room temperature using an artificial molecule with a small effective mass instead of a real Raman active molecule in the vicinity of plasmonic nanostructures [22]. It is an interesting mass-sensing system due to the large mass sensitivity of the mechanical resonator resulting from the large plasmon-phonon coupling [22–24].

The canonical model of cavity optomechanics can provide the ability to analyze the molecular plasmonic systems and subsequently investigate the effects of several parameters such as incident pump field, coupling strength, and

\*Corresponding author: [m-bagheri@phys.ui.ac.ir](mailto:m-bagheri@phys.ui.ac.ir)†Corresponding author: [Ehsan.amooghorban@sku.ac.ir](mailto:Ehsan.amooghorban@sku.ac.ir)

plasmonic damping rate on the transmission spectrum. However, the explicit dependence of these parameters upon the material and geometrical features of the system has been studied less analytically [25]. Establishing a formalism that prepares the physical ground to understand the influences of these parameters on the dynamics of the system and control the transmission peak height and shape of the probe beam would be practically useful. Therefore, as the main purpose of this study, we intend to include these features in the optomechanical formalism of the molecular plasmonic system.

Unlike the traditional method based on the first-principles approach to obtain the polarizability of a plasmonic nanostructure for the purpose of sensing [12], in the present work we start with the mode-selective quantization scheme to extract the optomechanical Hamiltonian describing the interaction between a plasmonic nanostructure and a suspended graphene nanoribbon (SGNR) [26,27]. This Hamiltonian contains the electromagnetic Green's tensor of the system through which dispersive and dissipative properties of plasmonic cavities enter the formalism. We then focus on two types of isotropic and anisotropic spherical plasmonic cavities and derive the multipolar polarizability from the Green's tensor of the system in the quasistatic approximation. In this way, we can analytically derive the optomechanical coupling strength, which includes the modal volume of the plasmonic subsystem. The modal volume is a crucial concept in the field of PCQED that quantifies the magnitude of the electric-field confinement. Although this parameter is not the geometrical volume it depends on the geometrical properties of the nanocavities [28,29].

This paper is organized as follows. In Sec. II we present the details of the mode-selective quantization method and then generalize this theoretical treatment to formulate a multimode optomechanical Hamiltonian expressing the interaction between plasmonic nanostructures and the SGNR. To further illustrate the flexibility of this method, in Sec. III we determine the explicit expression of the optomechanical strength and mode volume for coupling of the isotropic and anisotropic spherical plasmonic cavities to the SGNR. We subsequently obtain the transmission spectrum of the probe field related to the two aforementioned plasmonic systems for the sensing process at room temperature. In Sec. IV numerical results associated with the spectral function, optomechanical strength, and transmission spectrum are depicted and discussed. The paper is summarized by exploring optimal mass sensing in Sec. V. Details related to the mode-selective quantization, the free field Hamiltonian for the plasmonic subsystem, the quantum Langevin equations, and the Mie coefficients can be found in Appendixes A–D, respectively.

## II. THEORETICAL FRAMEWORK

In the present work we consider a composite plasmonic-molecule cavity optomechanical system, consisting of a clamped-clamped (doubly clamped) graphene nanoribbon in the vicinity of a spherical plasmonic nanocavity with radius  $R$  in the presence of two external fields. As shown in Fig. 1, the graphene nanoribbon lies in the  $xy$  plane and its axis is along the  $y$  direction. We suppose that the nanoribbon is located at the equilibrium distance  $r_m$  from the center of the spherical

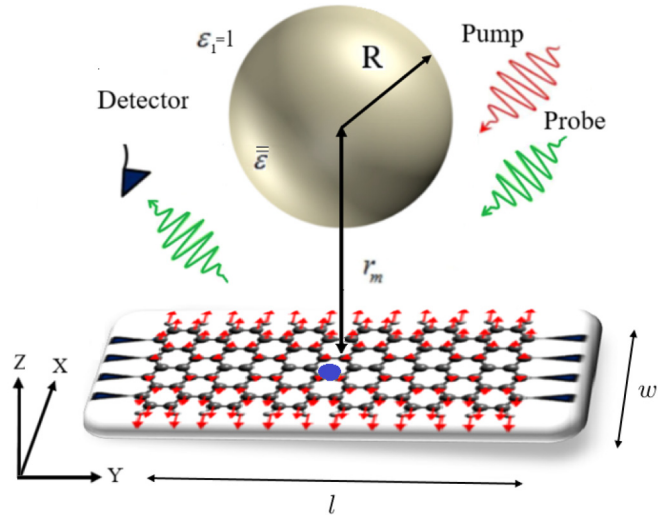


FIG. 1. (a) Schematic representation of the parametric interaction between the plasmonic cavity mode and nanoribbon Raman mode in the presence of a strong pump field and a weak probe field in vacuum. A doubly clamped graphene nanoribbon (armchair configuration) is located in the  $xy$  plane with periodicity in the  $y$  direction.

cavity at the origin and can vibrate in the horizontal direction. Here we consider the nanoribbon vibrations associated with the breathinglike mode, where all the atoms of the nanoribbon move in-plane along the ribbon width direction. This mode is Raman active due to the inversion symmetry of the atom-displacement pattern in the nanoribbon [30]. We can well characterize the vibrational mode of the SGNR by a harmonic oscillator with frequency  $\omega_m$ . The graphene nanoribbon has also been shown to support plasmonic modes which can be excited and tuned through special conditions [31,32]. Developments related to the electronic and plasmonic states of the graphene nanoribbon were addressed in Refs. [33–35]. The relative permittivity of the background medium is taken to be that of free space,  $\epsilon_1 = 1$ , and  $\bar{\epsilon}$  is the relative permittivity tensor of the spherical nanocavity.

The free Hamiltonian of the whole system is given by  $\hat{H}_{\text{free}} = \hat{H}_m + \hat{H}_p$ , in which the first term refers to the mechanical vibrations of the SGNR, i.e.,  $\hat{H}_m = \hbar\omega_m \hat{b}^\dagger \hat{b}$ . Here  $\hat{b}^\dagger$  ( $\hat{b}$ ) is the creation (annihilation) operator of the vibrational mode of the SGNR with the frequency  $\omega_m$ . In addition,  $\hat{H}_p$  is the free Hamiltonian of the plasmonic subsystem and describes the total energy of the electromagnetic field in a lossy plasmonic medium, so it can be written as

$$\hat{H}_p = \int d^3r \int_0^\infty d\omega \hbar\omega \hat{\mathbf{f}}^\dagger(\mathbf{r}, \omega) \cdot \hat{\mathbf{f}}(\mathbf{r}, \omega), \quad (1)$$

where the bosonic operators  $\hat{\mathbf{f}}^\dagger(\mathbf{r}, \omega)$  and  $\hat{\mathbf{f}}(\mathbf{r}, \omega)$  represent the collective excitations of the electromagnetic field and the medium with the commutation relation  $[\hat{f}_i(\mathbf{r}, \omega), \hat{f}_j^\dagger(\mathbf{r}', \omega')] = \delta_{ij} \delta(\mathbf{r} - \mathbf{r}') \delta(\omega - \omega')$  [36,37].

Let us model theoretically the parametric coupling between the optical modes of the plasmonic structure and the vibrational mode of the SGNR in the framework of molecular optomechanics [14]. This interaction Hamiltonian can be

described by the dipole interaction

$$\hat{H}_{\text{int}} = -\hat{\mathbf{P}}(\mathbf{r}_m) \cdot \hat{\mathbf{E}}(\mathbf{r}_m). \quad (2)$$

Here the induced Raman polarization  $\hat{\mathbf{P}}(\mathbf{r}_m)$  can be identified with the Raman polarizability tensor of the vibrational mode of the SGNR,  $\bar{\alpha}_R$ , as  $\hat{\mathbf{P}}(\mathbf{r}_m) = -\bar{\alpha}_R \cdot \hat{\mathbf{E}}(\mathbf{r}_m)$ . The Raman polarizability can be expressed in terms of the quantized displacement operator of the nanoribbon via the relation  $\bar{\alpha}_R = -\sqrt{\hbar/2\omega_m}(\hat{b} + \hat{b}^\dagger)\bar{\mathcal{R}}$ , wherein the second-rank Raman tensor  $\bar{\mathcal{R}}$  depends on the molecular structure and the bond nature of the SGNR [13].

Based on the canonical quantization scheme for the electromagnetic field in a dispersive and lossy medium [36–39], the positive-frequency part of the electric-field operator  $\hat{\mathbf{E}}^{(+)}$  can be written as

$$\hat{\mathbf{E}}^{(+)}(\mathbf{r}_m, \omega) = i \left( \frac{\omega^2}{c^2} \right) \int d^3r \sqrt{\frac{\hbar \bar{\epsilon}_I(\mathbf{r}, \omega)}{\pi \epsilon_0}} \bar{\mathbf{G}}(\mathbf{r}_m, \mathbf{r}, \omega) \cdot \hat{\mathbf{f}}(\mathbf{r}, \omega), \quad (3)$$

where  $\bar{\epsilon}_I(\mathbf{r}, \omega)$  is the imaginary part of the permittivity tensor of medium and  $\bar{\mathbf{G}}(\mathbf{r}_m, \mathbf{r}, \omega)$  is the classical Green's tensor satisfying the Helmholtz equation together with appropriate boundary conditions. The symmetry-related considerations in the point group theory for the graphene nanoribbon [40,41] along with the method of mode-selective quantization [26] allow us to derive a final discrete form of the Hamiltonian based on the new frequency-independent plasmonic operators  $\hat{a}_n(r_m)$  at the position of the nanoribbon as

$$\begin{aligned} \hat{H}_{\text{sys}} = & \sum_{n=1}^N \hbar \omega_n \hat{a}_n^\dagger(\mathbf{r}_m) \hat{a}_n(\mathbf{r}_m) + \hbar \omega_m \hat{b}^\dagger \hat{b} \\ & - 2\hbar(\hat{b} + \hat{b}^\dagger) \sum_{n=1}^N g_{\text{op},n} \hat{a}_n^\dagger(\mathbf{r}_m) \hat{a}_n(\mathbf{r}_m), \end{aligned} \quad (4)$$

where  $\omega_n$  describes the  $n$ th resonance frequency of the plasmonic cavity. Furthermore, the frequency-independent coupling function  $g_{\text{op},n} = 2|g_n(r_m)|^2$ , which is known as the optomechanical coupling strength, can be obtained by employing the spectral functions through the relation  $|g_n(r_m)|^2 = \int d\omega |k_n(r_m, \omega)|^2$ . More details on how this optomechanical coupling spectrum  $K_n = |k_n(r_m, \omega)|^2$  is generated and also the steps for obtaining this Hamiltonian are outlined in Appendixes A and B, respectively.

Mass sensing in the pump-probe technique requires examining the probe response of the SGNR [42,43]. To this purpose, the plasmonic subsystem is coherently driven by a strong pump field and a much weaker probe field, as shown in Fig. 1. Given this, we can obtain the total Hamiltonian of the system only by adding driving terms to the Hamiltonian  $\hat{H}_{\text{sys}}$ . For more convenience, we recast the total Hamiltonian in a reference frame rotating at the pump frequency, which yields

$$\begin{aligned} \hat{H}_{\text{tot}} = & \hbar \omega_m \hat{b}^\dagger \hat{b} + \sum_{n=1}^N \{ \hbar \Delta_n \hat{a}_n^\dagger(\mathbf{r}_m) \hat{a}_n(\mathbf{r}_m) \\ & - \hbar g_{\text{op},n} \hat{a}_n^\dagger(\mathbf{r}_m) \hat{a}_n(\mathbf{r}_m) (\hat{b}^\dagger + \hat{b}) \\ & - i\hbar \Omega_{\text{pr}} [\hat{a}_n(\mathbf{r}_m) e^{i\delta t} - \hat{a}_n^\dagger(\mathbf{r}_m) e^{-i\delta t}] \\ & - i\hbar \Omega_{\text{pu}} [\hat{a}_n(\mathbf{r}_m) - \hat{a}_n^\dagger(\mathbf{r}_m)] \}, \end{aligned} \quad (5)$$

where  $\Omega_{\text{pu}}$  and  $\Omega_{\text{pr}}$  are coherent driving coupling parameters related to the  $n$ th localized surface plasmonic (LSP<sub>*n*</sub>) mode with  $\Omega_i = \kappa_n \sqrt{\epsilon_0 V_{\text{eff}}/2\hbar\omega_n} E_{i,m}/2$  ( $i = \text{pu}, \text{pr}$ ) [44]. Here  $\kappa_n = \Gamma_n/2$  and  $E_{i,m}$  are the damping rate of the LSP<sub>*n*</sub> mode and the maximum near field scattered by the structure, respectively. The  $E_{i,m}$  can be written in terms of the plasmonic enhancement factor and incident pump field [45]. The parameter  $\Delta_n = \omega_n - \omega_{\text{pu}}$  is the detuning between the pump and the  $n$ th-mode plasmonic frequency; the detuning between the probe and pump field is defined as  $\delta = \omega_{\text{pr}} - \omega_{\text{pu}}$ .

Using the Heisenberg-Langevin approach [15,46], which includes dissipation and fluctuation mechanisms in the system, we can determine the time evolution of the plasmonic annihilation operator and the mean response of the mechanical subsystem. Since the incident probe field is much weaker than the pump field, we can employ the perturbation method to investigate the response of the probe field. Appendix C provides the derivation details of the output amplitude in the frequency of the probe field based on the pump-probe technique and input-output theory. These calculations help us build the output amplitude  $a_{n+, \text{out}} = \sqrt{2\kappa_n} a_{n+}$  or equivalently define the transmission of the probe beam as the ratio of the output and input amplitudes, i.e.,  $t(\omega_{\text{pr}}) = 1 - 2\kappa_n a_{n+}/\Omega_{\text{pr}}$  [15]. We will show that the  $a_{n+}$  contains all the information about the optomechanical strength and plasmonic damping rate of the  $n$ th plasmonic mode as well as the material and geometrical features, as will be seen in Eq. (C4). Determining the coupling strength in terms of the Green's tensor and using the procedure presented in the next section, we will analyze the probe response associated with several plasmonic subsystems.

### III. PLASMONIC CAVITIES

To illustrate how geometrical and material features of the plasmonic structure can modify the dynamics of the system and consequently the mass-sensing precision, in the present section we consider two cases and determine the explicit form of the optomechanical strength for them. We then study probe responses in each case.

#### A. Anisotropic spherical nanostructure optomechanically coupled to the SGNR

In the first case we consider a uniaxial anisotropic sphere illuminated by a plane wave. The form of the relative permittivity tensor for this anisotropic sphere is given by

$$\bar{\epsilon} = [(\epsilon_r - \epsilon_t)\hat{\mathbf{r}}\hat{\mathbf{r}} + \epsilon_t\bar{\mathbf{I}}], \quad (6)$$

where  $\bar{\mathbf{I}}$  is the unit dyad and  $\epsilon_r$  and  $\epsilon_t$  are the radial and tangential components of the permittivity tensor, respectively [47]. With the general form of the Green's tensor in hand and applying the symmetry consideration related to the radial anisotropic sphere, the scattering part of the Green's tensor for the tangential direction is simplified as

$$\begin{aligned} \bar{G}_{s,tt}^{(11)}(r_m, r_m) = & \frac{i\omega}{8\pi c} \sum_{n=0}^{\infty} (2n+1) \\ & \times \left[ B_N^{11} \left( \frac{\zeta'_n(k_1 r_m)}{k_1 r_m} \right)^2 + B_M^{11} [h_n^{(1)}(k_1 r_m)]^2 \right], \end{aligned} \quad (7)$$

where  $k_1 = \omega/c$ ,  $h_n^{(1)}(k_1 r_m)$  is the first-type of spherical Hankel function in the position of the nanoribbon,  $\zeta_n(k_1 r_m) = (k_1 r_m)h_n^{(1)}(k_1 r_m)$  is the spherical Riccati-Hankel function of the first kind, and the primed function refers to the derivative with respect to its argument. For a uniaxial anisotropic sphere with source and field points in the first layer, anisotropy effects appear only in the Mie coefficients  $B_l^{(11)} = -T_{l,12}^{(1)}/T_{l,11}^{(1)}$ , with  $l = N, M$ . Here  $T_{l,12}^{(1)}$  and  $T_{l,11}^{(1)}$  are elements of the transmission  $T$  matrix which are derived in Appendix D. If the radius of the sphere is very small compared to the wavelength of the incident field, we can restrict our attention to the QSA and simplify the Mie coefficients in this limit [48–51].

As described in Appendix D, the relevant Mie coefficient in our system is  $B_N^{(11)}$ . It is shown that in the QSA,  $B_N^{(11)}$  will be proportional to the modified quasistatic polarizability. This modified polarizability takes exactly the same form of polarizability as an isotropic sphere if we define an effective permittivity  $\varepsilon_{\text{eff}}^{\text{ani}}$  as

$$\varepsilon_{\text{eff}}^{\text{ani}} = \frac{\nu}{n} \varepsilon_r. \quad (8)$$

Here  $\nu = [n(n+1)\mathcal{A} + \frac{1}{4}]^{1/2} - \frac{1}{2}$ , in which the anisotropy ratio  $\mathcal{A}$  is defined as  $\mathcal{A} = \varepsilon_t/\varepsilon_r$  [47]. In what follows, we assume that both radial and tangential components of the permittivity tensor in Eq. (8) are given by the Drude-like model  $\varepsilon_i = \varepsilon_{\infty i} - \omega_{pi}^2/\omega(\omega + i\Gamma_{pi})$ , with  $i = t, r$ . We also suppose that the optical parameters of the two components obey the relations  $\omega_{pr}^2/\varepsilon_{\infty r} = \omega_{pt}^2/\varepsilon_{\infty t}$  and  $\Gamma_{pr} = \Gamma_{pt} = \Gamma_p$ . According to these assumptions, the effective permittivity  $\varepsilon_{\text{eff}}^{\text{ani}}$  takes a Drude-like form  $\varepsilon_{\text{eff}}^{\text{ani}} = \varepsilon_{\infty}^{\text{ani}} - (\omega_p^{\text{ani}})^2/\omega(\omega + i\Gamma_p)$ , in which the optical parameters are defined as follows:

$$\omega_p^{\text{ani}} = \left[ \left( \frac{n(n+1)\mathcal{A}_{\infty}}{n^2} + \frac{1}{4n^2} \right)^{1/2} - \frac{1}{2n} \right] \omega_{pr}, \quad (9a)$$

$$\varepsilon_{\infty}^{\text{ani}} = \left[ \left( \frac{n(n+1)\mathcal{A}_{\infty}}{n^2} + \frac{1}{4n^2} \right)^{1/2} - \frac{1}{2n} \right] \varepsilon_{\infty r}. \quad (9b)$$

Here  $\omega_p^{\text{ani}}$  and  $\varepsilon_{\infty}^{\text{ani}}$  represent the effective bulk plasmon frequency and the effective high-frequency limit of the dielectric function, respectively. According to the assumptions we made, the anisotropy ratio  $\mathcal{A}$  in the expression  $\varepsilon_{\text{eff}}^{\text{ani}}$  reduces to the constant parameter  $\mathcal{A}_{\infty} = \varepsilon_{\infty t}/\varepsilon_{\infty r}$ . Therefore, we can easily find the approximate imaginary part of the Green's tensor in the tangential direction near the resonance frequencies of the plasmonic cavity (for more details refer to Appendix D). Substituting this result into Eq. (A6), we get the approximate expression for the near-field frequency-dependent optomechanical coupling spectra as

$$K_n \approx \sqrt{\frac{\hbar}{2\omega_m}} \left( \frac{\bar{\mathcal{R}}\omega_n^{\text{ani}}}{16\pi\varepsilon_0} \right) \frac{n(n+1)(2n+1)R^{2n+1}}{[n\varepsilon_{\infty}^{\text{ani}} + (n+1)]r_m^{2n+4}} \times \frac{\Gamma_n^{\text{ani}}/2\pi}{(\omega_n^{\text{ani}} - \omega)^2 + (\Gamma_n^{\text{ani}}/2)^2}. \quad (10)$$

Here  $R$ ,  $r_m$ , and  $\bar{\mathcal{R}}$  represent the radius of the anisotropic sphere, the separation distance of the SGNR from the center of the sphere, and the diagonal elements of the Raman tensor  $\mathcal{R}_{ii}$  for  $i = x$ , respectively. The resonance frequency  $\omega_n^{\text{ani}}$  and

the total width  $\Gamma_n^{\text{ani}}$  corresponding to the  $n$ th localized surface plasmonic mode (LSP<sub>*n*</sub>) of the anisotropic sphere (effective sphere) are given in Appendix D. The coupling spectra  $K_n$  in Eq. (10) can be exploited to extract the modified optomechanical coupling strength of the anisotropic sphere as

$$g_{\text{op},n}^{\text{ani}} \approx \sqrt{\frac{\hbar}{2\omega_m}} (\bar{\mathcal{R}}\omega_n^{\text{ani}}) \frac{n(n+1)(2n+1)R^{2n+1}}{8\pi\varepsilon_0 [n\varepsilon_{\infty}^{\text{ani}} + (n+1)]r_m^{2n+4}}. \quad (11)$$

By defining the mode volume of the plasmonic nanocavity (anisotropic sphere) for the  $n$ th localized surface plasmonic mode as

$$V_n^{\text{ani}} = \frac{8\pi [n\varepsilon_{\infty}^{\text{ani}} + (n+1)]r_m^{2n+4}}{n(n+1)(2n+1)R^{2n+1}}, \quad (12)$$

the following expression for the parameter  $g_{\text{op},n}^{\text{ani}}$ , which was introduced in Ref. [12], is recovered:

$$g_{\text{op},n}^{\text{ani}} = \bar{\mathcal{R}}\sqrt{\hbar/2\omega_m} \left( \frac{\omega_n^{\text{ani}}}{\varepsilon_0 V_n^{\text{ani}}} \right). \quad (13)$$

## B. Isotropic spherical nanostructure optomechanically coupled to the SGNR

To demonstrate the role of anisotropy in the dynamics of the system and provide a quantitative comparison with its isotropic counterpart, we explore results for the second case of an isotropic spherical cavity, i.e., the limiting case  $\varepsilon_t = \varepsilon_r$ . In this limit, the modified Mie coefficients that are derived in Eqs. (D2a) and (D2b) reduce to the coefficients for the isotropic sphere, as developed in Ref. [52]. Furthermore, the permittivity function in Eq. (8) simplifies to the expression with Drude parameters  $\omega_p$  and  $\varepsilon_{\infty}$  for the isotropic sphere. So we can identify the optomechanical strength and modal volume for isotropic sphere by replacing the Drude-like parameters  $\omega_n^{\text{ani}}$  and  $\varepsilon_{\infty}^{\text{ani}}$  with their limiting parameters  $\omega_n$  and  $\varepsilon_{\infty}$  in Eqs. (11) and (12). In this way, the results in Eqs. (11) and (12) for  $\mathcal{A}_{\infty} = 1$  properly reduce to the corresponding expressions for the isotropic sphere. In Sec. IV we depict and compare the effects of these physical features on the sensing process for several plasmonic structures.

## IV. RESULTS AND DISCUSSION

### A. Optomechanical coupling strength

In this section we numerically study the behavior of the optomechanical coupling spectra and strengths for the interaction between each plasmonic nanostructure and the SGNR. We compare the obtained results for different plasmonic structures. We then explore the effects of the material, geometrical, and modal parameters on the system dynamics and consequently the sensing process.

First of all, we list the physical parameters of the subsystems. Consider a graphene armchair nanoribbon of dimensions  $l \approx 22$  nm and  $w \approx 22$  nm with the frequency of the breathinglike mode  $\omega_m \approx 470$  GHz [53,54] and the total mass  $m \approx 3 \times 10^{-22}$  kg [55,56]. The quality factor of the Raman active mode drastically decreases at room temperature. This results in a damping rate of  $\gamma = 1.9$  GHz. We set the quantum yield of the nanoribbon  $\eta = 0.01$  and assume that the square of the Raman tensor element  $\bar{\mathcal{R}}$  is of order

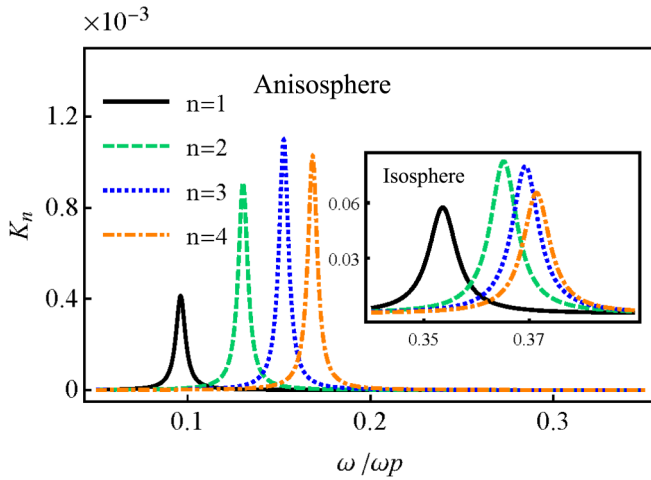


FIG. 2. Optomechanical coupling spectra versus  $\omega/\omega_p$  for coupling of the SGNR to the first four  $LSP_n$  modes of the anisotropic nanosphere with  $\mathcal{A}_\infty = 0.01$ . The inset shows a close-up of the spectra for the silver sphere nanocavity. Here we set  $r_m = 14$  nm and  $R = 10$  nm. The other material parameters are  $\omega_p = 0.19$  pHz,  $\omega_m = 470$  GHz, and  $\gamma = 1.9$  GHz.

$10^3$  ( $\text{\AA}^4 \text{amu}^{-1}$ ) [13]. For the isotropic nanocavity, we take into account a silver nanosphere of radius  $R = 10$  nm placed at a distance of  $r_m = 14$  nm from the graphene nanoribbon and characterize their dissipative and dispersive properties by the Drude model with typical parameters:  $\omega_p = 1.9$  pHz,  $\Gamma_p = 0.012$  pHz, and  $\varepsilon_\infty = 6$  [57–59]. For the anisotropic nanocavity in which both radial and tangential components of the permittivity tensor are described by the Drude-like model, we also choose the above material parameters for the radial component along with a variable anisotropy ratio. Using these parameters and Eqs. (9a) and (9b), we can easily get the effective material parameters  $\varepsilon_\infty^{\text{ani}}$  and  $\omega_p^{\text{ani}}$ .

We can now analyze the coupling of the SGNR to the plasmonic nanocavity modes. The inset of Fig. 2 represents the Lorentzian coupling spectra  $K_n$  for coupling of the first four  $LSP_n$  modes of the silver nanosphere to the SGNR as a function of a dimensionless frequency  $\omega/\omega_p$ . We observe that the Lorentzian peaks associated with the spectral coupling functions  $K_n$  start to overlap each other by increasing the order of multipolar coupling  $n$ . Thus, it seems that the silver sphere nanocavity is not a suitable structure for mass sensing since spectral functions cannot be resolved properly and overlap noticeably, especially for higher mode couplings.

Results for anisotropic spherical nanocavity are plotted in Fig. 2, manifesting the role of anisotropy in the dynamics of the system. As it is evident, spectral functions are slightly redshifted and narrowed by decreasing the anisotropy ratio from  $\mathcal{A}_\infty = 1$  to 0.01. Furthermore, there is no significant spectral interference compared to the isotropic nanosphere case. Therefore, by manipulating the anisotropy ratio, the Lorentzian curves are split from each other and the position of peaks can be tuned. All of these features become practically useful in the sensing process and will be addressed in more detail later.

The optomechanical coupling strength corresponding to the interaction between the SGNR and several multipolar

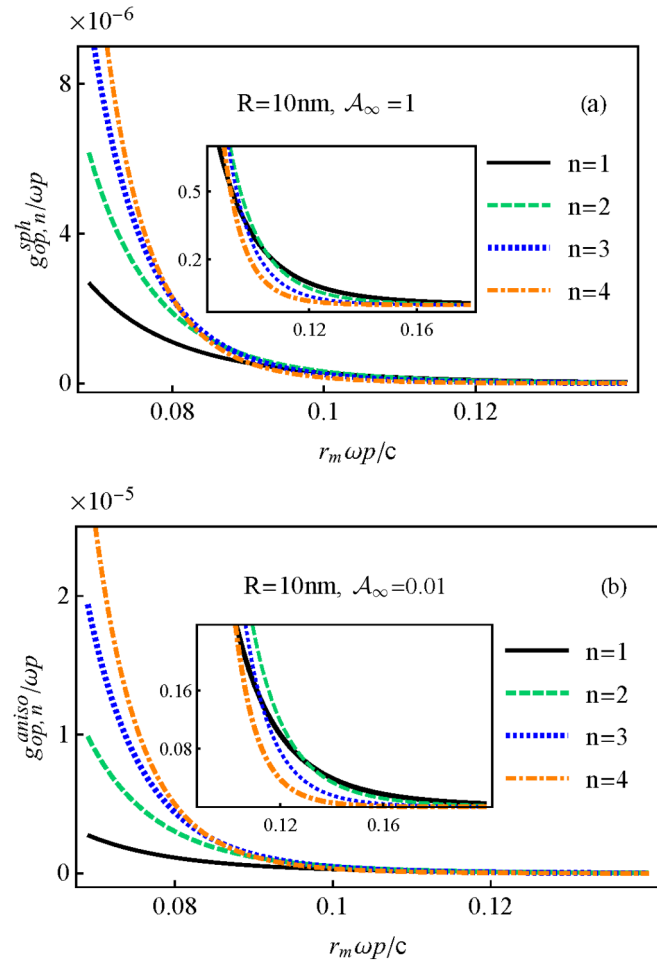


FIG. 3. Optomechanical coupling strength versus  $r_m \omega_p/c$  for the interaction between the SGNR and the first four  $LSP_n$  modes of (a) the silver nanosphere and (b) the anisotropic nanosphere. The values for the parameters are the same as those in Fig. 2. The insets show close-ups of the panels within the range  $r_m \approx 0.084c/\omega_p - 0.19c/\omega_p$ . Scaled separation distances are approximately equivalent to the interval distance  $r_m = 11\text{--}22$  nm.

modes of the isotropic and anisotropic nanospheres is illustrated as a function of the dimensionless distance  $r_m \omega_p/c$  in Figs. 3(a) and 3(b), respectively. As expected, for two plasmonic nanocavities the optomechanical coupling strength is greater at smaller separation distances for all  $LSP$  modes. We see clearly that the interaction between the plasmonic modes of the anisotropic nanosphere and the SGNR results in larger values for the coupling strength regardless of the magnitude of  $n$  in Fig. 3(b). Comparing the behavior of the several multipolar couplings in Figs. 3(a) and 3(b), we find that for separation distances up to  $r_m \approx 19$  nm, coupling of the SGNR to the higher-order plasmonic modes plays an essential role in the dynamics of the system. However, the dipolar coupling (black solid curves) becomes dominant for large distances.

## B. Mass sensing

Having explained the behavior of the coupling strength, we now present numerical results for mass sensing through the pump-probe technique [60–62]. Our purpose is to

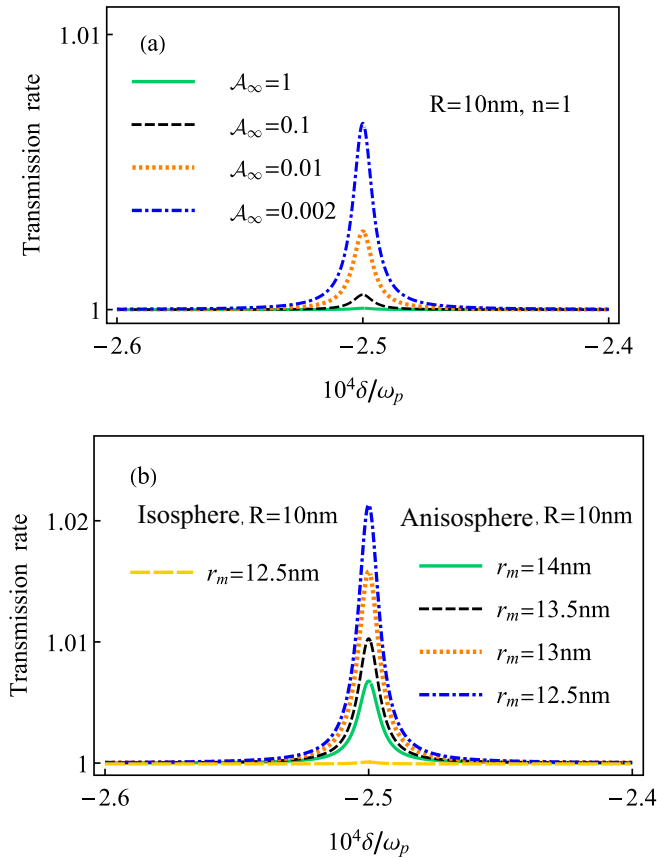


FIG. 4. Transmission rate versus  $\delta/\omega_p$  for dipolar coupling of the SGNR to (a) the silver nanocavity and (b) the anisotropic nanosphere with  $\mathcal{A}_\infty = 0.002$ . The values for the other parameters are the same as those in Fig. 2.

manipulate the geometrical and material features of the spherical nanostructures to see how the probe spectrum is affected at room temperature. Using Eqs. (C4) and (C5), we can obtain the transmission spectrum of the probe field. In Fig. 4(a) we illustrate the probe-field transmission spectra for the optomechanical couplings of the isotropic and anisotropic nanospheres to the SGNR in terms of the probe-cavity detuning  $\delta$  at fixed separation distance  $r_m = 14\text{nm}$ . Note that here  $\delta$  is specifically defined as  $\delta = \omega_1 - \omega_{pr}$ , which corresponds to the dipolar coupling.

We analyze the results for  $\mathcal{A}_\infty = 0.1$  (black dashed curve),  $\mathcal{A}_\infty = 0.01$  (orange dotted curve), and  $\mathcal{A}_\infty = 0.002$  (blue dot-dashed curve). We see that the strength of the transmission peak is enhanced by decreasing  $\mathcal{A}_\infty$  from 1 for the isotropic silver nanosphere (green solid curve) to a smaller value for the anisotropic nanosphere. This is related to the role of the mode volume as well as the damping rate of plasmonic nanocavities. Traditional CQED investigates the dynamics of the atom-field interaction by exploring the influence of the cavity quality factor, while in PCQED the key parameter is the mode volume [9,46]. Plasmonic nanocavities confine electromagnetic energy beyond the classical diffraction limit, resulting in small mode volumes. Since the coupling strength is inversely proportional to the mode volume, the nanostructures with smaller mode volume provide larger coupling strength and

consequently higher transmission peak. When the anisotropy ratio decreases from the value  $\mathcal{A}_\infty = 1$  to 0.01, the enhancement of the optomechanical coupling strength occurs due to mode volume reduction. This is verified by the plots in Figs. 3(a) and 3(b), in which the optomechanical coupling strength of the SGNR to the anisotropic nanocavity modes with  $\mathcal{A}_\infty = 0.01$  is stronger than the silver sphere modes regardless of the order of interaction.

It is worth noting that further reduction of the anisotropy ratio leads to smaller optomechanical coupling strengths compared to the value of 0.01 (here the figure is not presented for the sake of brevity). However, in contrast, the redshift of the resonance frequencies leads to the enhancement of the coupling functions between the plasmonic field and the classical incident fields ( $\Omega_{pu}$  and  $\Omega_{pr}$ ). These features provide a higher transmission peak for the smaller anisotropy ratio, as shown in Fig. 4(a).

For nanostructures with a small radius, the plasmonic damping rate comprises two terms: the Joule term that accounts for electron scattering losses and the radiative damping term [49,50]. Having estimated the damping rates related to the dipolar mode of the two plasmonic nanocavities, we find that the total damping rate of the anisotropic nanosphere becomes slightly smaller than the damping rate of the silver sphere nanocavity due to the smaller contribution of the radiative damping term.

In Fig. 4(b) we illustrate the influence of the separation distance  $r_m$  on the probe transmission spectrum for dipolar coupling of the anisotropic nanosphere to the SGNR. Here the results are depicted for a fixed anisotropy ratio  $\mathcal{A}_\infty = 0.002$ . As expected, when the SGNR gets closer to the surface of the anisotropic nanosphere, the intensity of the transmission peak is enhanced slightly, which makes it easier to detect for sensing purposes. For the SGNR placed 4 nm away from the anisotropic nanosphere surface, the result is shown with the green solid curve in Fig. 4(b). We observe that the peak intensity for the anisotropic nanosphere at a farther distance is greater than that for the isotropic nanosphere at a shorter distance (yellow long-dashed curve). Notice that for distances less than  $r_m = 11\text{nm}$ , nonlocal effects become increasingly pronounced, which are beyond the scope of the present study.

So far, we have examined the effects of the anisotropy ratio and separation distance on the transmission spectrum. In Fig. 5(a) we compare the behavior of the spectrum peaks for the coupling of the SGNR to the three first  $LSP_n$  modes of the anisotropic nanosphere. Here we set  $\mathcal{A}_\infty = 0.002$  and  $r_m = 12.5\text{nm}$ . Results indicate that close to the surface of the spherical nanocavity, higher-order mode coupling exhibits a higher peak intensity.

The sensing process with a weak incident pump field provides a suitable platform for the exploration of living organisms' features. Therefore, in Fig. 5(b) we depict the transmission peak strength for the probe field in terms of the incident pump intensity of the order  $I_{pu} \approx 10\text{ kW/cm}^2$ . The corresponding results for higher intensities are plotted in the inset of Fig. 5(b).

The extremely small size of the SGNR makes physical properties greatly sensitive to the perturbations originating from the external force and mass adsorbed on it. Based on the relationship between mass changes of the graphene

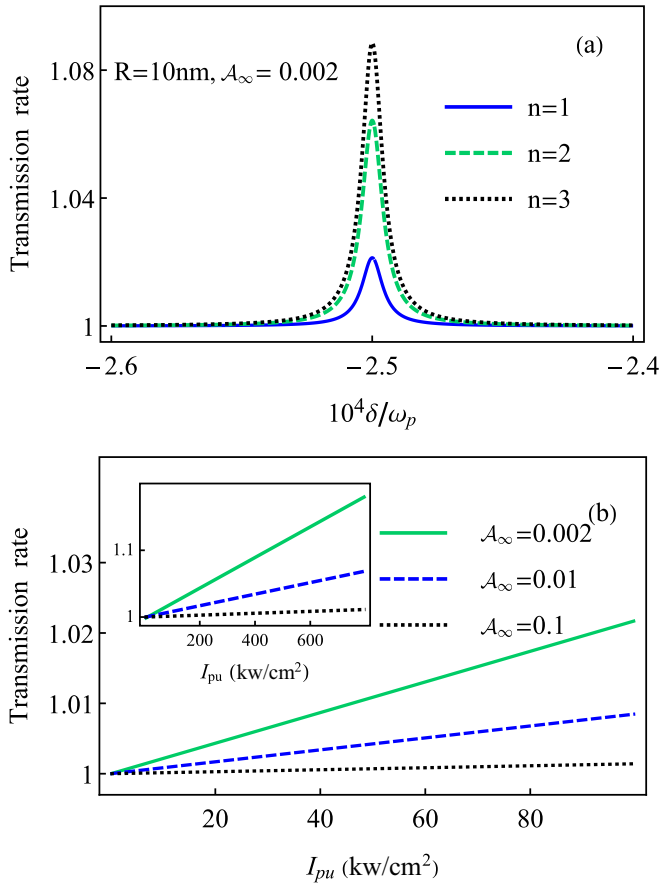


FIG. 5. (a) Transmission rate versus  $\delta/\omega_p$  for coupling the SGNR to several multipolar modes of the anisotropic sphere with  $R = 10$  nm and  $r_m = 12.5$  nm. (b) Transmission rate versus incident pump intensity. The other parameters are  $\omega_p = 0.19$  pHz,  $\omega_m = 470$  GHz, and  $\gamma = 1.9$  GHz.

nanoribbon and its frequency shift, one can perform a sensing process through the relation  $\Delta m = 2m\Delta\omega/\omega_m$  [53]. In the pump-probe scheme, the frequency shift induced by the molecular species loaded onto the nanoribbon surface is monitored. A minimal measurable mass depends on the bandwidth of the absorption spectrum. To understand the accuracy of mass sensing in this system, we make a numerical estimation in the following.

As it is evident from the black dotted curve in Fig. 5(a), the octupolar coupling results in the highest peak for the transmission spectrum at the separation distance  $r_m = 12.5$  nm when the anisotropic nanosphere is illuminated with the incident pump intensity  $I_{pu} \approx 400$  kW/cm<sup>2</sup>. Therefore, we can estimate the full width at half maximum of the probe spectrum for the black dotted curve in Fig. 5(a), which is  $\Delta\omega \approx 0.18$  GHz. The calculation indicates that the minimum resolution for mass sensing takes the value  $\Delta m \approx 1.2 \times 10^{-24}$  kg. For lower intensities of order  $I_{pu} \approx 40$  kW/cm<sup>2</sup>, the height of the transmission peak decreases to the approximate value 0.01. However, the accuracy of mass sensing becomes almost the same as before.

Notice that the analytical method introduced here can be generalized to include a variety of plasmonic nanocav-

ities as the optical subsystem. For multilayered plasmonic nanostructures, optical properties can be adjusted more accurately due to the tunable geometrical and material parameters of these structures. This feature makes plasmonic nanocavities attractive for sensing applications since the optomechanical coupling strength, as well as the plasmonic damping rate, can be adjusted more effectively through manipulating optical features of these multilayered nanostructures. The tunable plasmonic damping rate and coupling strength affect the width and height of the probe transmission spectrum, respectively. Thus, an anisotropic spherical nanoshell (core) in combination with the metallic core (nanoshell), which can provide mass sensing with higher precision, is a promising subject for future study.

In the end, the nanomechanical subsystem may be affected by the thermomechanical and momentum exchange noises [63], as well the Casimir force. The contribution of the first two effects is negligible at room temperature (see Ref. [63]), while an approximate estimation of the Casimir force to examine its effect on the sensing process is needed. Bimonte derived a semianalytic formula  $F_c = -(\pi^3 \hbar c R / 360 h^3)$  for the spherical plate Casimir force, in which  $R$  is the radius of the spherical structure and  $h$  represents the separation distance between the plate and the surface of the metallic sphere [64]. For parameter values  $R = 10$  nm and  $h = 3$  nm, the Casimir force takes the value  $F_c = 9 \times 10^{-27}$  N. In another study, Biels and Agarwal investigated the Casimir-Polder force between a gold nanoparticle and a single sheet of pristine graphene in detail [65]. They showed that although the graphene sheet behaves like a perfect metal for distances larger than the thermal wavelength, for small distances the Casimir-Polder force is relatively small compared to the values of the ideal metal case and depends on the Fermi level of the graphene sheet. Bearing this in mind, it is clear that the weight of the minimum measurable mass would still be comparable to the Casimir force.

## V. CONCLUSION

In this paper we have investigated the anisotropy effects of the nanocavity on mass sensing in the molecular plasmonic system. To do so, we have presented a formalism that allows us to manipulate the transmission spectrum of the probe field for mass sensing through the pump-probe technique. In this manner, the molecular plasmonic system was mapped onto the cavity optomechanical model [13,14] and then the mode-selective quantization scheme presented in Ref. [26] was extended to formulate a multimode Hamiltonian of the optomechanical system.

It was shown that the geometrical, material, and modal considerations, which are relevant to the plasmonic subsystem, are contained in the Hamiltonian through the electromagnetic Green's tensor. We found the explicit form of the optomechanical coupling strength, the parametric interaction between the plasmonic mode, and the Raman active mode of the SGNR in terms of the symmetrical and geometrical properties of the graphene nanoribbon and plasmonic nanocavity. Taking symmetry properties of the nanoribbon into account, we determined the coupling spectral function and optomechanical strength for some spherical plasmonic structures by

extracting their Green's tensors. We showed that an anisotropic nanocavity with a small anisotropy ratio is more suitable for the sensing process. Furthermore, the manipulation of anisotropy features of the plasmonic nanocavity made it possible to reduce mode volume (enhance optomechanical strength) and damping rate for optimal mass sensing. We then illustrated transmission spectra for two cases of plasmonic nanostructures. The results indicated an enhancement in the transmission peak corresponding to the anisotropic nanocavity and verified its superiority over the isotropic one for sensing applications.

In a traditional optomechanical system, a high- $Q$  microcavity at cryogenic temperature is needed to accurately perform mass sensing. Recently, mass sensing with precision of order  $10^{-26}$  kg was performed in molecular plasmonic systems with low- $Q$  plasmonic nanocavities (cylindrical dimer) at room temperature [22]. Of course, we can attribute this high efficiency to the small mode volume of the plasmonic nanocavity as well as a controversial frequency considered for the breathinglike mode of the graphene nanoribbon. Unlike the previous work developed by Liu and Zhu, as a main purpose of this paper, we have presented an analytical method to explicitly calculate the mode volume and damping rate of plasmonic modes for different plasmonic nanocavities. Of course, improving the accuracy of the current mass-sensing device and achieving the highest accuracy by engineering the plasmonic multilayered nanostructures is worth further consideration.

#### APPENDIX A: MODE-SELECTIVE QUANTIZATION APPROACH

The Green's tensor contains all modal information of the plasmonic structure. Following the method developed in Refs. [26,27], we consider a spherical geometry for which the Green's tensor can be decomposed as a sum over the discrete modes (multipole expansion with spherical symmetry)

$$\bar{\mathbf{G}}(\mathbf{r}_m, \mathbf{r}, \omega) = \sum_{n=1}^{\infty} \bar{\mathbf{G}}_n(\mathbf{r}_m, \mathbf{r}, \omega), \quad (\text{A1})$$

where the index  $n$  represents the radial harmonic index and  $\bar{\mathbf{G}}_n(\mathbf{r}_m, \mathbf{r}, \omega)$  contains contribution of the LSP $_n$  (dipolar plasmon for  $n = 1$ , quadrupole plasmon for  $n = 2$ , etc.). Similar to the Green's tensor, the electric-field operator associated with the plasmonic structure can be written in terms of the several multipole components

$$\hat{\mathbf{E}}(\mathbf{r}_m, \omega) = \sum_{n=1}^{\infty} \hat{\mathbf{E}}_n(\mathbf{r}_m, \omega). \quad (\text{A2})$$

The component  $\hat{\mathbf{E}}_n(\mathbf{r}_m, \omega)$  describes the electric-field operator associated with the LSP $_n$ . Point group theory tells us that the fundamental vibration of the nanoribbon with the breathinglike displacement of the phonon mode has  $A_g$  symmetry (diagonal Raman tensor) just for special scattering patterns of a doubly clamped nanoribbon [30,40]. If this condition is met, the spectral decomposition of the electric-field operator in the frequency domain leads to the simplified form of the

interaction Hamiltonian in Eq. (2) as

$$\begin{aligned} \hat{H}_{\text{int}} = & -\sqrt{\frac{\hbar}{2\omega_m}}(\hat{b} + \hat{b}^\dagger) \iint d\omega d\omega' \mathcal{R}_{ii} \\ & \times \{\hat{E}_i^{(-)}(\mathbf{r}_m, \omega) \hat{E}_i^{(+)}(\mathbf{r}_m, \omega') \\ & + \hat{E}_i^{(+)}(\mathbf{r}_m, \omega) \hat{E}_i^{(-)}(\mathbf{r}_m, \omega')\}, \end{aligned} \quad (\text{A3})$$

where  $\mathcal{R}_{ii}$  are diagonal elements of the SGNR Raman tensor with  $i = x, y, z$  (here Einstein's sum convention is used). In the above Hamiltonian, we have neglected two terms in Eq. (A3) since they do not satisfy the energy conservation. Up to now, we have considered the localized plasmon polaritons in a continuous band description. However, the dynamics of the composite system is based on the excitation of the LSP modes of the spherical nanostructure by an external pump laser and optomechanical coupling to the vibrational mode of the mechanical subsystem. Therefore, based on the scheme of the mode-selective quantization developed in Refs. [26,27] along with the Gram-Schmidt orthogonalization procedure, we suppose that  $N$  discrete modes participate in the coupling process. In this manner, we introduce the mode-selective bosonic annihilation operator as

$$\hat{a}_n(\mathbf{r}_m, \omega) = \sqrt{\mathcal{R}_{ii}/(2\omega_m\hbar)}^{1/2} \alpha_n(\omega) \hat{e}_i \hat{E}_{n,i}^{(+)}(\mathbf{r}_m, \omega), \quad (\text{A4})$$

where  $\hat{e}_i$  ( $i = 1, 2, 3$ ) are the Cartesian unit vectors. The operator  $\hat{a}_n(\mathbf{r}_m, \omega)$  is associated with the LSP $_n$  mode at the position of the nanoribbon and can be excited by the external laser at a given position of the mechanical resonator. It is worth noting that the introduced mode-selective bosonic operators satisfy the usual bosonic commutation relation  $[\hat{a}_n(\mathbf{r}_m, \omega), \hat{a}_m^\dagger(\mathbf{r}_m, \omega')] = \delta(\omega - \omega') \delta_{nm}$ , provided  $\alpha_n(\omega)$  is given by the relation  $|\alpha_n(\omega)|^2 = 1/|k_n(r, \omega)|^2$  with

$$\begin{aligned} |k_n(\mathbf{r}, \omega)|^2 = & (\mathcal{R}_{ii} k_1^2 / \pi \epsilon_0) \\ & \times \sqrt{\hbar/2\omega_m} \hat{e}_i \cdot [\text{Im} \bar{\mathbf{G}}_{n,s}(\mathbf{r}_m, \mathbf{r}, \omega)] \cdot \hat{e}_i. \end{aligned} \quad (\text{A5})$$

Employing the quantization method, the interaction part of the Hamiltonian can be obtained in terms of the frequency-dependent bosonic operator  $\hat{a}_n(\mathbf{r}_m, \omega)$  and the spectral coupling functions  $k_{n,m}(\mathbf{r}_m, \omega)$ . To completely perform the mode-selective quantization scheme and obtain the final effective Hamiltonian, we need to determine the explicit form of the spectral function. Considerations related to the symmetrical and vibrational properties of the phonon modes, as well as the electromagnetic Green's tensor, help us identify the form of  $k_n(\mathbf{r}_m, \omega)$ . For an armchair graphene ribbon in the  $xy$  plane with periodicity along the  $y$  direction, the  $A_g$  mode is Raman active for geometry  $(zXXz)$ . Here  $zz(XX)$  represent the propagation (polarizations) directions of the incident and scattered light, respectively [30,40,41]. Based on the properties of the  $A_g$  symmetrized Raman tensor, we only need diagonal components of the scattering Green's tensor  $\bar{\mathbf{G}}_{s,ii}^{(11)}(\mathbf{r}_m, \mathbf{r}_m)$  with  $i = x$ . By applying symmetry arguments, the optomechanical coupling spectra  $K_n = |k_n(\mathbf{r}_m, \omega)|^2$  is obtained as

$$K_n = \left( \frac{\mathcal{R}_{ii} k_1^2}{\pi \epsilon_1} \right) \sqrt{\hbar/2\omega_m} \text{Im}[\bar{\mathbf{G}}_{n,s}(\mathbf{r}_m, \mathbf{r}_m, \omega)]_{ii}. \quad (\text{A6})$$

Finding the general form of spectral function, we can go one step further and introduce new frequency-independent plasmonic operators  $\hat{a}_n(\mathbf{r}_m)$  at the position of the nanoribbon

$$\hat{a}_n(\mathbf{r}_m) = \beta_n \int d\omega k_n(\mathbf{r}_m, \omega) \hat{a}(\mathbf{r}_m, \omega). \quad (\text{A7})$$

The coefficient  $\beta_m$  is determined through the relation  $|\beta_m|^2 = 1/\int d\omega |k_n(\mathbf{r}_m, \omega)|^2$  so that these newly defined plasmonic operators satisfy the bosonic commutation relation as  $[\hat{a}_n(\mathbf{r}_m), \hat{a}_m^\dagger(\mathbf{r}_m)] = \delta_{nm}$ . The effective Hamiltonian is obtained by integrating over the angular frequency to establish a set of  $N$  discrete modes.

### APPENDIX B: DERIVATION OF THE FREE FIELD HAMILTONIAN FOR THE PLASMONIC SUBSYSTEM

In the following we indicate the main steps toward deriving the quantum Langevin equation and free field Hamiltonian of the plasmonic subsystem. Based on the methods developed in Refs. [26,27], we can decompose the plasmonic part of the free field Hamiltonian into the predefined bright mode and a set of continuous noninteracting orthogonal dark modes

$$\hat{\mathbf{d}}(\mathbf{r}, \omega) = \hat{\mathbf{f}}(\mathbf{r}, \omega) - \sum_{n=1}^N [\hat{\mathbf{f}}(\mathbf{r}, \omega), \hat{a}_n^\dagger(\mathbf{r}_m, \omega)] \hat{a}_n(\mathbf{r}_m, \omega). \quad (\text{B1})$$

Since dark modes have independent dynamics and will not affect the dynamics of the bright modes, after some algebraic calculations, we arrive at the relation

$$\int d^3r \hat{\mathbf{f}}^\dagger(\mathbf{r}, \omega) \cdot \hat{\mathbf{f}}(\mathbf{r}, \omega) = \sum_{n=1}^N \hat{a}_n^\dagger(\mathbf{r}_m, \omega) \hat{a}_n(\mathbf{r}_m, \omega) + \int d^3r \hat{\mathbf{d}}^\dagger(\mathbf{r}, \omega) \cdot \hat{\mathbf{d}}(\mathbf{r}, \omega). \quad (\text{B2})$$

The term related to the free Hamiltonian of dark modes can be omitted since it plays no role in the dynamics of the system. To determine the plasmonic part of the Hamiltonian based on the frequency-independent bosonic operator, we first start with the quantum Langevin equation for the new plasmonic operator  $d\hat{a}_n(\mathbf{r}_m)/dt = [\hat{a}_n(\mathbf{r}_m), \hat{H}_0]/i\hbar$  in which the Hamiltonian  $\hat{H}_0$  is defined as

$$\hat{H}_0 = \int d\omega \hbar\omega \sum_{n=1}^N \hat{a}_n^\dagger(\mathbf{r}_m, \omega) \hat{a}_n(\mathbf{r}_m, \omega). \quad (\text{B3})$$

Here we have used the definition of the bosonic annihilation operator  $\hat{a}_n(\mathbf{r}_m, \omega)$  in the position of the SGNR to rewrite the Langevin equation as

$$\dot{\hat{a}}_n(\mathbf{r}_m) = - \int d\omega \omega k_n(\mathbf{r}_m, \omega) \hat{a}_n(\mathbf{r}_m, \omega) / g_n(\mathbf{r}_m). \quad (\text{B4})$$

Equation (B4) is not yet a closed equation for  $\hat{a}_n(\mathbf{r}_m)$ , since there is an additional integral kernel apart from the definition of the operators  $\hat{a}_n(\mathbf{r}_m)$ . To get a closed form, we subtract and add the term  $(-\omega_n + i\Gamma_n/2)$  to the integral kernel and then use the relation

$$k_n(\mathbf{r}_m, \omega) = \sqrt{\frac{\Gamma_n}{2\pi}} \frac{ig_n(\mathbf{r}_m)}{(\omega - \omega_n) + i\Gamma_n/2}. \quad (\text{B5})$$

We arrive at the following quantum Langevin equation that includes the quantum noise and dissipation terms:

$$\dot{\hat{a}}_n(\mathbf{r}_m) = -i\omega_n \hat{a}_n(\mathbf{r}_m) - \left(\frac{\Gamma_n}{2}\right) \hat{a}_n(\mathbf{r}_m) + \hat{F}_n(\mathbf{r}_m). \quad (\text{B6})$$

Here the quantum noise is defined as  $\hat{F}_n(\mathbf{r}_m) = -i \int d\omega \sqrt{\Gamma_n/2\pi} \hat{a}_n(\mathbf{r}_m, \omega)$ . Equation (B6) now can be considered as the quantum Langevin equation for the new plasmonic operator with respect to the Hamiltonian  $\hat{H}_p = \sum_{n=1}^N \hbar\omega_n \hat{a}_n^\dagger(\mathbf{r}_m) \hat{a}_n(\mathbf{r}_m)$ . In the end, incorporating the nanoribbon Hamiltonian and its interaction term in the equation of motion, we get

$$\dot{\hat{a}}_n(\mathbf{r}_m) = \frac{[\hat{a}_n(\mathbf{r}_m), \hat{H}_{\text{sys}}]}{i\hbar} - \left(\frac{\Gamma_n}{2}\right) \hat{a}_n(\mathbf{r}_m) + \hat{F}_n(\mathbf{r}_m). \quad (\text{B7})$$

### APPENDIX C: LINEARIZATION OF THE QUANTUM LANGEVIN EQUATIONS IN THE PUMP-PROBE TECHNIQUE

Heisenberg equations of motion for the plasmonic annihilation operator and the mean response of the mechanical subsystem  $\hat{n} = \hat{b} + \hat{b}^\dagger$  are given by

$$\dot{\hat{a}}_n(\mathbf{r}_m) = -(i\Delta_n + \kappa_n) \hat{a}_n(\mathbf{r}_m) + ig_{\text{op},n} \hat{a}_n(\mathbf{r}_m) \hat{n} + \Omega_{\text{pu}} + \Omega_{\text{pr}} \exp(-i\delta t) + \hat{F}_n(\mathbf{r}_m), \quad (\text{C1a})$$

$$\dot{\hat{n}} + \gamma \hat{n} = -\omega_m^2 \hat{n} + 2\omega_m g_{\text{op},n} \hat{a}_n^\dagger(\mathbf{r}_m) \hat{a}_n(\mathbf{r}_m) + \hat{\xi}(t). \quad (\text{C1b})$$

Equation (C1a) represents the dynamics of the  $n$ th plasmonic mode. The correlations associated with the quantum vacuum fluctuations of the plasmonic cavity modes are fully characterized by the  $\delta$ -correlation functions as developed in Refs. [15,46]. In Eq. (C1b),  $\gamma$  and  $\hat{\xi}(t)$  represent the damping rate and Brownian noise of the SGNR, respectively. Here the SGNR is affected by a Brownian stochastic force with zero mean value and the correlation function that is given in Ref. [15]. Since the incident probe field is much weaker than the pump field, we employ the perturbation method to investigate the optical properties of the system [22]. In the pump-probe technique, the Heisenberg operators can be decomposed as the sum of a steady-state mean value and a small fluctuation with zero mean value, i.e.,  $\hat{a}_n(t) = \bar{a}_n + \delta\hat{a}_n(t)$  and  $\hat{n}(t) = \bar{n} + \delta\hat{n}(t)$ , with the steady-state mean values  $\bar{a}_n = \hat{a}_{n0}$  and  $\bar{n} = n_0$ . To obtain the steady-state solutions of the operators, we set the time derivatives of operators in Eqs. (C1a) and (C1b) equal to zero, which yields  $a_{n0} = \Omega_{\text{pu}}/[i(\Delta_n - g_{\text{op},n}n_0) + \kappa_n]$ , where  $n_0 = 2g_{\text{op},n}\omega_0/\omega_m$  with  $\omega_0 = |a_{n0}|^2$ .

Inserting these definitions in Eqs. (C1a) and (C1b) and neglecting the terms  $\delta\hat{a}_n(t)\delta\hat{n}(t)$ , quantum Langevin equations governing the time evolution of the fluctuation operators can be derived as

$$\delta\dot{\hat{a}}_n(\mathbf{r}_m) = -(i\Delta_n + \kappa_n) \delta\hat{a}_n(\mathbf{r}_m) + ic_0 g_{\text{op},n} \delta\hat{n} + in_0 g_{\text{op},n} \delta\hat{a}_n(\mathbf{r}_m) + \Omega_{\text{pr}} e^{-i\delta t} + \hat{F}_n(\mathbf{r}_m), \quad (\text{C2a})$$

$$\delta\dot{\hat{n}} = -\gamma \delta\hat{n} - \omega_m^2 \delta\hat{n} + 2c_0 \omega_m g_{\text{op},n} \delta\hat{a}_n^\dagger(\mathbf{r}_m) + 2c_0^* \omega_m g_{\text{op},n} \delta\hat{a}_n(\mathbf{r}_m) + \hat{\xi}(t). \quad (\text{C2b})$$

We identify all fluctuation operators with their expectation values and eliminate the noise terms. To solve these sets of equations, we use the following ansatz in the rotating frame:

$$\langle \delta \hat{a}_n(\mathbf{r}_m) \rangle = a_{n+} \exp(-i\delta t) + a_{n-} \exp(i\delta t), \quad (\text{C3a})$$

$$\langle \delta \hat{n} \rangle = n_+ \exp(-i\delta t) + n_- \exp(i\delta t). \quad (\text{C3b})$$

Now we substitute these equations into Eqs. (C2a) and (C2b), then equate the terms with the same time dependence, and finally find the solution for  $a_{n+}$ :

$$a_{n+} = \frac{\Omega_{\text{pr}}[w(x_n - y_n) + z_n]}{w(x_n^2 - y_n^2) + 2y_n z_n}. \quad (\text{C4})$$

Equation (C4) is given in the lowest order in  $\Omega_{\text{pu}}$  but to all orders of  $\Omega_{\text{pr}}$ . Here the parameter  $w$  and functions  $z_n$ ,  $y_n$ , and  $x_n$  are defined as  $w = -(\delta^2 + i\gamma\delta + \omega_m^2)$ ,  $z_n = 2i(\omega_m\omega_0)g_{\text{op},n}^2$ ,  $y_n = i\Delta_n - in_0g_{\text{op},n}$ , and  $x_n = \kappa_n - i\delta$ , respectively. To investigate the optical response of the system via the output field, we employ the input-output relation  $\hat{a}_{n,\text{out}}(t) + \hat{a}_{n,\text{in}}(t) = \sqrt{2\kappa_n}\hat{a}_n(t)$  [15]. Given that the mean value of the input operator  $\hat{a}_{n,\text{in}}(t)$  is equal to zero, we obtain

$$\begin{aligned} \langle \hat{a}_{n,\text{out}}(t) \rangle &= a_{n0,\text{out}} + a_{n+,\text{out}}e^{-i\delta t} + a_{n-,\text{out}}e^{i\delta t} \\ &= \sqrt{2\kappa_n}(a_{n0} + a_{n+}e^{-i\delta t} + a_{n-}e^{i\delta t}). \end{aligned} \quad (\text{C5})$$

#### APPENDIX D: MIE COEFFICIENTS OF THE GREEN'S TENSOR FOR AN ANISOTROPIC SPHERE

The electromagnetic Green's tensor for a radial anisotropic sphere has been extracted previously in Ref. [47]. When the field and the source points are located in the first layer, the electromagnetic Green's tensor can be separated into two parts of the vacuum and the scattering. The former describes the contribution of the direct waves from the source in the free space. The latter represents the contribution of the multiple transmission and reflection waves that occur due to interfaces. The role of the anisotropy of the plasmonic structure is included in the Green's tensor through a noninteger order  $\nu = [n(n+1)\mathcal{A} + \frac{1}{4}]^{1/2} - \frac{1}{2}$  and an anisotropy ratio  $\mathcal{A} = \varepsilon_t/\varepsilon_r$ . By imposing the boundary conditions and employing the recursive algorithm method, all the unknown scattering Mie coefficients can be determined. For the spherical structure under study, the Mie coefficients can be obtained in terms of the transmission  $T$ -matrix elements as

$$B_l^{(11)} = -\frac{T_{l,12}^{(1)}}{T_{l,11}^{(1)}}, \quad (\text{D1})$$

with  $l = N, M$ . For  $l = N$ , the elements of the transformation matrix are given by [47]

$$T_{N,11}^{(1)} = \frac{\psi_\nu(k_t R)\zeta'_\nu(k_t R)/\eta_t - \zeta_\nu(k_t R)\psi'_\nu(k_t R)/\eta_1}{\psi_\nu(k_t R)\zeta'_\nu(k_t R)/\eta_t - \zeta_\nu(k_t R)\psi'_\nu(k_t R)/\eta_1}, \quad (\text{D2a})$$

$$T_{N,12}^{(1)} = \frac{\psi_\nu(k_t R)\psi'_\nu(k_t R)/\eta_t - \psi_\nu(k_t R)\psi'_\nu(k_t R)/\eta_1}{\psi_\nu(k_t R)\zeta'_\nu(k_t R)/\eta_t - \zeta_\nu(k_t R)\psi'_\nu(k_t R)/\eta_1}, \quad (\text{D2b})$$

where  $k_t^2 = \omega^2\varepsilon_t\mu_t/c^2$ ,  $\eta_t = \sqrt{\mu_t/\varepsilon_t}$ , and  $\psi_\nu(z)$  and  $\zeta_\nu(z)$  represent the spherical Riccati-Bessel and Riccati-Hankel functions, respectively,

$$\psi_\nu(z) = zj_\nu(z), \quad (\text{D3a})$$

$$\zeta_\nu(z) = zh_\nu^{(1)}(z). \quad (\text{D3b})$$

These functions and their derivatives in the QSA are defined as

$$\psi_\nu(z) \sim \frac{z^{\nu+1}}{2^{\nu+1}\Gamma(\nu + \frac{3}{2})}, \quad (\text{D4a})$$

$$\zeta_\nu(z) \sim \frac{(-i)2^\nu(-1)^{\nu+1}\sqrt{\pi}}{z^\nu\Gamma(-\nu + \frac{1}{2})}, \quad (\text{D4b})$$

$$\psi'_\nu(z) \sim \frac{\sqrt{\pi}(\nu+1)z^\nu}{2^{\nu+1}\Gamma(\nu + \frac{3}{2})}, \quad (\text{D4c})$$

$$\zeta'_\nu(z) \sim \frac{(-i)2^\nu(-1)^{\nu+1}\sqrt{\pi}(-\nu)}{z^\nu\Gamma(-\nu + \frac{1}{2})}. \quad (\text{D4d})$$

Now, by substituting Eqs. (D4a)–(D4d) into Eqs. (D2a) and (D2b), the Mie coefficient  $B_N^{(11)}$  is given by

$$B_N^{(11)} = \frac{i(k_1 R)^{2n+1}[(n+1)\varepsilon_t - (\nu+1)]}{(2n-1)!!(2n+1)!![n\varepsilon_t + (\nu+1)]}. \quad (\text{D5})$$

In the first layer, i.e., the free space, the noninteger order  $\nu$  reduces to the integer value  $n$ . Moreover, the imaginary part of the Mie coefficient  $B_M^{(11)}$  vanishes, so it has no contribution to the optomechanical coupling spectra in the QSA. By defining the effective permittivity as

$$\varepsilon_{\text{eff}}^{\text{ani}} = \varepsilon_r \left[ \left( \frac{n(n+1)\varepsilon_t}{\varepsilon_r n^2} + \frac{1}{4n^2} \right)^{1/2} - \frac{1}{2n} \right], \quad (\text{D6})$$

the polarizability of the anisotropic sphere takes exactly the same form as the polarizability of an effective sphere

$$\alpha^{\text{ani}} = \frac{n(\varepsilon_{\text{eff}}^{\text{ani}} - 1)R^{2n+1}}{n\varepsilon_{\text{eff}}^{\text{ani}} + (n+1)}, \quad (\text{D7})$$

with effective Drude-like parameters that were introduced in Sec. III. Now we can identify the imaginary part of the tangential Green's tensor and the spectral function.

The resonance frequency  $\omega_n^{\text{ani}}$ , which corresponds to the LSP<sub>*n*</sub> mode of the effective sphere in Eq. (10), can be expressed as

$$\omega_n^{\text{ani}} = \omega_{p,\text{eff}}^{\text{ani}} \sqrt{n/[n\varepsilon_{\infty,\text{eff}}^{\text{ani}} + (n+1)]} \quad (\text{D8})$$

and the total width is  $\Gamma_n^{\text{ani}} = \Gamma_p^{\text{ani}} + \Gamma_{\text{nrad}}^{\text{ani}}$ . The first term in  $\Gamma_n^{\text{ani}}$  indicates the Ohmic loss and the second term represents radiation damping rate  $\Gamma_{\text{nrad}}^{\text{ani}}$ , which is given by

$$\Gamma_{\text{nrad}}^{\text{ani}} = \frac{\omega_n^{\text{ani}}(2n+1)(n+1)(k_n R)^{2n+1}}{n[n\varepsilon_{\infty,\text{eff}}^{\text{ani}} + (n+1)](2n-1)!!(2n+1)!}. \quad (\text{D9})$$

This term is added to the Ohmic loss to take into account the variation of the electric field over the particle size [49,50]. It is obvious that for  $\varepsilon_t = \varepsilon_r$ , the spherical Bessel and Hankel functions of the order  $\nu$  and Drude-like parameters reduce to

the spherical Bessel and Hankel functions of the order  $n$  and the corresponding Drude parameters for the isotropic sphere,

respectively. In this limit, the obtained Mie coefficients would be the same as those for the isotropic sphere [52].

- 
- [1] M. S. Tame, K. R. McEnery, Ş. K. Özdemir, J. Lee, S. A. Maier, and M. S. Kim, Quantum plasmonics, *Nat. Phys.* **9**, 329 (2013).
- [2] T. Neuman, R. Esteban, D. Casanova, F. J. García-Vidal, and J. Aizpurua, Coupling of molecular emitters and plasmonic cavities beyond the point-dipole approximation, *Nano Lett.* **18**, 2358 (2018).
- [3] J. T. Hugall, A. Singh, and N. F. van Hulst, Plasmonic cavity coupling, *ACS Photon.* **5**, 43 (2018).
- [4] M. I. Stockman, K. Kneipp, S. I. Bozhevolnyi, S. Saha, A. Dutta, J. Ndukaife, N. Kinsey, H. Reddy, U. Guler, V. M. Shalaev, and A. Boltasseva, Roadmap on plasmonics, *J. Opt.* **20**, 043001 (2018).
- [5] R. Chikkaraddy, B. De Nijs, F. Benz, S. J. Barrow, O. A. Scherman, E. Rosta, A. Demetriadou, P. Fox, O. Hess, and J. J. Baumberg, Single-molecule strong coupling at room temperature in plasmonic nanocavities, *Nature (London)* **535**, 127 (2016).
- [6] D. Xu, X. Xiong, L. Wu, X.-F. Ren, C. E. Png, G.-C. Guo, and Y.-F. Xiao, Quantum plasmonics: New opportunity in fundamental and applied photonics, *Adv. Opt. Photon.* **10**, 703 (2018).
- [7] J. Zhang, L. Zhang, and W. Xu, Surface plasmon polaritons: Physics and applications, *J. Phys. D* **45**, 113001 (2012).
- [8] A. Balytis, Y. Nishijima, S. Krishnamoorthy, A. Kuchmizhak, P. R. Stoddart, R. Petrukevicius, and S. Juodkazis, From fundamental toward applied SERS: Shared principles and divergent approaches, *Adv. Opt. Mater.* **6**, 1800292 (2018).
- [9] P. Ginzburg, Cavity quantum electrodynamics in application to plasmonics and metamaterials, *Rev. Phys.* **1**, 120 (2016).
- [10] S.-Y. Ding, E.-M. You, Z.-Q. Tian, and M. Moskovits, Electromagnetic theories of surface-enhanced Raman spectroscopy, *Chem. Soc. Rev.* **46**, 4042 (2017).
- [11] M. Fleischmann, P. J. Hendra, and A. J. McQuillan, Raman spectra of pyridine adsorbed at a silver electrode, *Chem. Phys. Lett.* **26**, 163 (1974).
- [12] Y. D. Yin, L. Gao, and C. W. Qiu, Electromagnetic theory of tunable SERS manipulated with spherical anisotropy in coated nanoparticles, *Phys. Chem C* **115**, 8893 (2011).
- [13] P. Roelli, C. Galland, N. Piro, and T. J. Kippenberg, Molecular cavity optomechanics as a theory of plasmon-enhanced Raman scattering, *Nat. Nanotechnol.* **11**, 164 (2016).
- [14] M. K. Schmidt, R. Esteban, F. Benz, J. J. Baumberg, and J. Aizpurua, Linking classical and molecular optomechanics descriptions of SERS, *Faraday Discuss.* **205**, 31 (2017).
- [15] M. Aspelmeyer, T. J. Kippenberg, and F. Marquardt, Cavity optomechanics, *Rev. Mod. Phys.* **86**, 1391 (2014).
- [16] M. K. Schmidt and J. Aizpurua, Nanocavities: Optomechanics goes molecular, *Nat. Nanotechnol.* **11**, 114 (2016).
- [17] M. K. Schmidt, R. Esteban, A. González-Tudela, G. Giedke, and J. Aizpurua, Quantum mechanical description of Raman scattering from molecules in plasmonic cavities, *ACS Nano* **10**, 6291 (2016).
- [18] J. Liu and K. D. Zhu, Coupled quantum molecular cavity optomechanics with surface plasmon enhancement, *Photon. Res.* **5**, 450 (2017).
- [19] S. M. Ashrafi, R. Malekfar, A. R. Bahrapour, and J. Feist, Optomechanical heat transfer between molecules in a nanoplasmonic cavity, *Phys. Rev. A* **100**, 013826 (2019).
- [20] M. K. Dezfouli, R. Gordon, and S. Hughes, Molecular optomechanics in the anharmonic cavity-QED regime using hybrid metal-dielectric cavity modes, *ACS Photon.* **6**, 1400 (2019).
- [21] Y. Zhang, J. Aizpurua, and R. Esteban, Optomechanical collective effects in surface-enhanced Raman scattering from many molecules, *ACS Photon.* **7**, 1676 (2020).
- [22] J. Liu and K. D. Zhu, Room temperature optical mass sensor with an artificial molecular structure based on surface plasmon optomechanics, *Photon. Res.* **6**, 867 (2018).
- [23] J. J. Li and K. D. Zhu, All-optical mass sensing with coupled mechanical resonator systems, *Phys. Rep.* **525**, 223 (2013).
- [24] H. J. Chen and K. D. Zhu, Graphene-based nanoresonator with applications in optical transistor and mass sensing, *Sensors* **14**, 16740 (2014).
- [25] M. K. Dezfouli and S. Hughes, Quantum optics model of surface-enhanced Raman spectroscopy for arbitrarily shaped plasmonic resonators, *ACS Photon.* **4**, 1245 (2017).
- [26] D. Dzsotjan, B. Rousseaux, H. R. Jauslin, G. C. des Francs, C. Couteau, and S. Guerin, Mode-selective quantization and multimodal effective models for spherically layered systems, *Phys. Rev. A* **94**, 023818 (2016).
- [27] A. Castellini, H. R. Jauslin, B. Rousseaux, D. Dzsotjan, G. C. des Francs, A. Messina, and S. Guérin, Quantum plasmonics with multi-emitters: Application to stimulated Raman adiabatic passage, *Eur. Phys. J. D* **72**, 223 (2018).
- [28] P. T. Kristensen and S. Hughes, Modes and mode volumes of leaky optical cavities and plasmonic nanoresonators, *ACS Photon.* **1**, 2 (2014).
- [29] S. Huang, T. Ming, Y. Lin, X. Ling, Q. Ruan, T. Palacios, J. Wang, M. Dresselhaus, and J. Kong, Ultrasmall mode volumes in plasmonic cavities of nanoparticle-on-mirror structures, *Small* **12**, 5190 (2016).
- [30] R. Gillen, M. Mohr, and J. Maultzsch, Raman active modes in graphene nanoribbons, *Phys. Status Solidi B* **247**, 2941 (2010).
- [31] D. Legrand, L. O. Le Cunff, A. Bruyant, R. Salas-Montiel, Z. Liu, B. K. Tay, T. Maurer, and R. Bachelot, Surface plasmons in suspended graphene: Launching with in-plane gold nanoantenna and propagation properties, *Opt. Express* **25**, 17306 (2017).
- [32] S. Thongrattanasiri, A. Manjavacas, and F. J. García de Abajo, Quantum finite-size effects in graphene plasmons, *ACS Nano* **6**, 1766 (2012).
- [33] L. Brey and H. A. Fertig, Elementary electronic excitations in graphene nanoribbons, *Phys. Rev. B* **75**, 125434 (2007).
- [34] D. R. Andersen and H. L. Raza, Plasmon dispersion in semimetallic armchair graphene nanoribbons, *Phys. Rev. B* **85**, 075425 (2012).
- [35] A. Iurov, L. Zhemchuzhna, G. Gumbs, D. Huang, P. Fekete, F. Anwar, D. Dahal, and N. Weekes, Tailoring plasmon excitations in  $\alpha$ - $T_3$  armchair nanoribbons, *Sci. Rep.* **11**, 20577 (2021).
- [36] T. Gruner and D. G. Welsch, Green-function approach to the radiation-field quantization for homogeneous and

- inhomogeneous Kramers-Kronig dielectrics, *Phys. Rev. A* **53**, 1818 (1996).
- [37] H. T. Dung, L. Knoll, and D.-G. Welsch, Spontaneous decay in the presence of dispersing and absorbing bodies: General theory and application to a spherical cavity, *Phys. Rev. A* **62**, 053804 (2000).
- [38] M. Morshed Behbahani, E. Amooghorban, and A. Mahdifar, Spontaneous emission and the operation of invisibility cloaks, *Phys. Rev. A* **94**, 013854 (2016).
- [39] F. Kheirandish, M. Amooshahi, and E. Amooghorban, *Proceedings of the Third International Meeting on Frontiers in Physics, Kuala Lumpur, 2009*, edited by S. P. Chia, K. Ratnavelu, and M. R. Muhamad, AIP Conf. Proc. No. 1150 (AIP, Melville, 2009), p. 416.
- [40] R. Gillen, M. Mohr, and J. Maultzsch, Symmetry properties of vibrational modes in graphene nanoribbons, *Phys. Rev. B* **81**, 205426 (2010).
- [41] R. Saito, M. Furukawa, G. Dresselhaus, and M. S. Dresselhaus, Raman spectra of graphene ribbons, *J. Phys: Condens. Matter* **22**, 334203 (2010).
- [42] D. Yan, K.-H. Gu, C.-N. Ren, L. Chen, and J.-H. Wu, Pump-probe response sensitive to atomic excitation in a hybrid optomechanical system, *J. Phys. B* **51**, 155003 (2018).
- [43] Y.-P. Gao, T.-J. Wang, C. Cao, S.-C. Mi, D. Yang, Y. Zhang, and C. Wang, Effective mass sensing using optomechanically induced transparency in microresonator system, *IEEE Photon. J.* **9**, 2639045 (2016).
- [44] R. Esteban, J. Aizpurua, and G. W. Bryant, Strong coupling of single emitters interacting with phononic infrared antennae, *New J. Phys.* **16**, 013052 (2014).
- [45] G. C. des Francs, J. Barthes, A. Bouhelier, J. C. Weeber, A. Dereux, A. Cuche, and C. Girard, Plasmonic Purcell factor and coupling efficiency to surface plasmons. Implications for addressing and controlling optical nanosources, *J. Opt.* **18**, 094005 (2016).
- [46] M. O. Scully and M. S. Zubairy, *Quantum Optics* (Cambridge University Press, Cambridge, 1997).
- [47] C. W. Qiu, S. Zouhdi, and A. Razek, Modified spherical wave functions with anisotropy ratio: Application to the analysis of scattering by multilayered anisotropic shells, *IEEE Trans. Antennas Propag.* **55**, 3515 (2007).
- [48] *Handbook of Mathematical Functions*, edited by M. Abramowitz and I. A. Stegun (Dover, New York, 1972).
- [49] C. F. Bohren and D. R. Huffman, *Absorption and Scattering of Light by Small Particles* (Wiley-Interscience, New York, 1998).
- [50] G. C. Des Francs, Molecule non-radiative coupling to a metallic nanosphere: An optical theorem treatment, *Int. J. Mol. Sci.* **10**, 3931 (2009).
- [51] G. Colas des Francs, S. Derom, R. Vincent, A. Bouhelier, and A. Dereux, Mie plasmons: Modes volumes, quality factors, and coupling strengths (purcell factor) to a dipolar emitter, *Int. J. Opt.* **2012**, 1 (2012).
- [52] L.-W. Li, P.-S. Kooi, M.-S. Leong, and T.-S. Yee, Electromagnetic dyadic Green's function in spherically multilayered media, *IEEE Trans. Microw. Theory Tech.* **42**, 2302 (1994).
- [53] D. Liu, C. Daniels, V. Meunier, A. G. Every, and D. Tomanek, In plane breathing and shear modes in low dimensional nanostructures, *Carbon* **157**, 364 (2020).
- [54] J. Zhou, and J. Dong, Radial breathing-like mode of wide carbon nanoribbon, *Phys Lett. A.* **372**, 7183 (2008).
- [55] G. Kalosakas, N. N. Lathiotakis, and K. Papagelis, Width dependent elastic properties of graphene nanoribbons, *Materials* **14**, 5042 (2021).
- [56] H. Hiura, M. V. Lee, A. V. Tyurnina, and K. Tsukagoshi, Liquid phase growth of graphene on silicon carbide, *Carbon* **50**, 5076 (2012).
- [57] J. Hakami, L. Wang, and M. S. Zubairy, Spectral properties of a strongly coupled quantum-dot-metal-nanoparticle system, *Phys. Rev. A* **89**, 053835 (2014).
- [58] C. Van Vlack, P. T. Kristensen, and S. Hughes, Spontaneous emission spectra and quantum light-matter interactions from a strongly coupled quantum dot metal-nanoparticle system, *Phys. Rev. B* **85**, 075303 (2012).
- [59] P. B. Johnson and R. W. Christy, Optical constants of the noble metals, *Phys. Rev. B* **6**, 4370 (1972).
- [60] J. J. Li and K. D. Zhu, A scheme for measuring vibrational frequency and coupling strength in a coupled nanomechanical resonator-quantum dot system, *Appl. Phys. Lett.* **94**, 063116 (2009).
- [61] W. He, J.-J. Li, and K.-D. Zhu, Coupling-rate determination based on radiation-pressure-induced normal mode splitting in cavity optomechanical systems, *Opt. Lett.* **35**, 339 (2010).
- [62] H.-J. Chen and K.-D. Zhu, Surface plasmon enhanced sensitive detection for possible signature of majorana fermions via a hybrid semiconductor quantum Dot-Metal nanoparticle system, *Sci. Rep.* **5**, 13518 (2015).
- [63] K. L. Ekinici, Y. T. Yang, and M. L. Roukes, Ultimate limits to inertial mass sensing based upon nanoelectromechanical systems, *J. Appl. Phys.* **95**, 2682 (2004).
- [64] G. Bimonte, Going beyond PFA: A precise formula for the sphere-plate Casimir force, *Europhys. Lett.* **118**, 20002 (2017).
- [65] S. A. Biehs and G. S. Agarwal, Anisotropy enhancement of the Casimir-Polder force between a nanoparticle and graphene, *Phys. Rev. A* **90**, 042510 (2014).